Spectroscopic factors and asymptotic normalization coefficients for $0p$-shell nuclei: Recent updates

N. K. Timofeyuk
Department of Physics, University of Surrey, Guildford, Surrey GU2 7XH, United Kingdom
(Received 12 August 2013; revised manuscript received 10 September 2013; published 14 October 2013)

Extended tables are presented for spectroscopic factors, asymptotic normalization coefficients and rms radii of one-nucleon overlap functions for $0p$-shell nuclei calculated in the source term approach using shell model wave functions. The tabulated data includes both new results and updates on previously published values. They are compared with recent results obtained in *ab initio* calculations, and with experimental data, where available. The reduction of spectroscopic factors with respect to traditional shell model values as well as its neutron-proton asymmetry is also discussed.

DOI: 10.1103/PhysRevC.88.044315 PACS number(s): 21.10.Jx, 27.20.+n

I. INTRODUCTION

Experimental evidence accumulated over decades of studies shows that cross sections of nucleon removal reactions are smaller than predictions made by reaction theories that use single-particle wave functions and shell model spectroscopic factors (SFs) [1–5]. This is referred to as reduction of spectroscopic strength and is often interpreted as reduction of spectroscopic factors. Almost all knockout and transfer experiments claim a reduction of the spectroscopic strength by $\sim$0.55 for stable nuclei (except in Ref. [6] where no reduction is seen for standard neutron potential well parametrization). However, the reduction of spectroscopic strength in neutron- or proton-rich nuclei is controversial: knockout experiments show evidence of asymmetry in removing a weakly bound neutron (proton) and a deeply bound proton (neutron) from the same target [4,7,8] while transfer experiments claim limited neutron-proton asymmetry in SFs reduction [5,9,10].

The reduction of spectroscopic strength is backed by *ab initio* calculations within Green function Monte Carlo (GFMC) [11], variational Monte Carlo (VMC) [11–13], no-core shell model (NCSM) [12], coupled-cluster method (CCM) [14], and self-consistent Green's function method (SCGFM) [10,15,16]. These methods predict smaller spectroscopic factors than either the independent particle model (IPM) or the traditional shell model does. They also show neutron-proton asymmetry in deviation of spectroscopic factors from IPM or from the shell model which is, however, not as large as the one observed in knockout experiments but can be larger than the one claimed by transfer reactions studies.

Whether the experimental and/or predicted SFs should be compared to the shell model ones needs further clarification. The shell model spectroscopic factors are calculated from the wave functions Ψ_P obtained in a restricted model space P usually given by $0\hbar\omega$. Ψ_P are obtained from Hamiltonians H_{PP} that contain effective rather than realistic NN interactions, as required by the missing model spaces Q. The missing model spaces also require renormalization of any other operators sandwiched by Ψ_P. Such a renormalization is made, for example, for electromagnetic operators by using effective charges. However, no renormalization is ever made when spectroscopic factors are calculated by widely used shell model codes such as OXBASH, NUSHELL, or ANTOIN. Therefore, it is not surprising that the shell model spectroscopic factors obtained in this way differ either from those obtained in more advanced *ab initio* approaches involving much larger model spaces or from the experimental values.

It has been shown that the easiest way to include missing shell model spaces into the calculation of the overlap functions is to solve the inhomogeneous equation they satisfy [17–20]. The source term for this equation can be calculated using Ψ_P. Then a proper choice of the effective interaction between the removed nucleon and the nucleons of the daughter nucleus will account for the missing model spaces Q. The resulting spectroscopic factors calculated as norms of the overlap functions are more suitable for comparison with results from other approaches and with experimental data.

Whether the experimental determination of spectroscopic factors is really possible deserves a further comment. It has been shown in Ref. [21] that spectroscopic factors are not invariant under finite-range unitary transformations and, therefore, are not observables. The exact reaction amplitudes are not parametrized in terms of the spectroscopic factors and nuclear reactions in the exact approach cannot provide a tool to determine spectroscopic factor. In practice, the spectroscopic factors are found on the assumption that the radial part of the overlap is known, which is not always true. On the contrary, asymptotic normalization coefficients (ANCs), which are the amplitudes of the asymptotic tails of the overlap functions [22], are invariant under finite-range unitary transformations and thus can be observable [21]. The source term approach (STA) of [18,20] easily predicts ANCs that can be directly compared to experimental values where available.

This paper updates available knowledge on spectroscopic factors and ANCs for $0p$-shell nuclei. The necessity of such an update follows from a growing number of one-nucleon removal experiments, performed in the last few years since the publication of STA results for SFs and ANCs in [17,18], and from more *ab initio* results for overlap functions published over the same period. Also, some inaccuracies have been noticed in the previous publication of ANCs and SFs in [17,18] that originate from errors in calculating the contributions from noncentral components of the NN interactions. These inaccuracies as well as misprints are corrected in the present paper and the tables of SFs and ANCs are significantly extended to cover the cases of recent experimental and theoretical interest. Section II reviews the STA formalism and

provides the updated values of ANCs, SFs, and rms radii of the overlap integrals. It also points at neutron-proton asymmetry in SF reduction from the original shell model calculations. The ANCs and spectroscopic factors from STA are compared with the calculations of *ab initio* approaches and with experimental data in Secs. III and IV, respectively. The conclusions are given in Sec. V and new analytical expressions for the STA two-body matrix elements are presented in the Appendix.

II. OVERLAP FUNCTIONS IN THE SOURCE TERM APPROACH

The radial overlap function $I_{lj}(r)$ with orbital momentum l and angular momentum j is defined as an overlap integral between the wave functions Ψ_{J_B} and Ψ_{J_A} of two neighboring nuclei $B=A-1$ and A with the total spin J_B and J_A:

$$I_{lj}(r) = A^{1/2}\langle[[Y_l(\hat{\boldsymbol{r}})\otimes\chi^{\tau}_{1/2}]_j\otimes\Psi_{J_B}]_{J_A}|\Psi_{J_A}\rangle. \quad (1)$$

Here the integration is carried out over $3A-6$ independent coordinates describing the internal structure of nucleus B, r is the distance between the center of mass of B and the removed nucleon, Y_l is the spherical function and $\chi^{\tau}_{1/2}$ is the spin-isospin function of the removed nucleon with isospin projection τ. The coefficient $A^{1/2}$ comes from antisymmetrization. The spectroscopic factor S_{lj} is the norm of $I_{lj}(r)$:

$$S_{lj} = \int_0^\infty dr\, r^2 I^2_{lj}(r). \quad (2)$$

At $r\to\infty$, the overlap $I_{lj}(r)$ has the well-known form

$$I_{lj}(r) \approx C_{lj}\frac{W_{-\eta,l+1/2}(2\kappa r)}{r}, \quad r\to\infty, \quad (3)$$

where C_{lj} is the ANC, W is the Whittaker function, $\eta = Z_B Z_N e^2\mu/\hbar^2\kappa$, Z_B and Z_N are the charge of B, and the removed nucleon N, respectively, $\kappa=(2\mu\varepsilon/\hbar^2)^{1/2}$, $\varepsilon=E_A-E_B$, E_A and E_B are the binding energies of nuclei A and B, respectively, and μ is the reduced mass.

In the STA, the overlap function is obtained as the solution

$$I_{lj}(r) = A^{\frac{1}{2}}\left\langle\left[\left[\frac{G_l(r,r')}{rr'}Y_l(\hat{\boldsymbol{r}}')\otimes\chi^{\tau}_{\frac{1}{2}}\right]_j\otimes\Psi_{J_B}\right]_{J_A}||\hat{\mathcal{V}}||\Psi_{J_A}\right\rangle, \quad (4)$$

of the inhomogeneous equation $(T_l+V^0_c+\varepsilon)I_{lj}(r) = -U_{lj}(r)$ with the source term $U_{lj}(r)$ [17,18,20]. In Eq. (4) the integration over r' is implied and $G_l(r,r')$ is the Green's function for a bound nucleon in the field of a point charge Z_B,

$$G_l(r,r') = -\frac{2\mu}{\hbar^2\kappa}e^{-\pi i(l+1+\eta)/2}F_l(i\kappa r_<)W_{-\eta,l+1/2}(2\kappa r_>), \quad (5)$$

corresponding to the momentum $i\kappa$. Here F is the regular Coulomb function. Also, $\hat{\mathcal{V}}=\sum_{i=1}^{B}v^{\rm eff}_{iA}-V^0_c$, and V^0_c is the point Coulomb interaction between the valence nucleon and B. The source term $U_{lj}(r)$ is given by the same expression as Eq. (4) but in which the function $G_l(r,r')/(rr')$ and the integration over r' is absent. Equation (4) generates an $I_{lj}(r)$ which automatically has the correct asymptotic shape when the experimental value of ε is used, whatever Ψ_{J_A} and Ψ_{J_B} are. Following Refs. [17,18,20], these functions are represented by the harmonic oscillator wave functions with the oscillator radius derived from electron scattering in Ref. [23]. The wrong tails of the oscillator wave functions are not important since, due to the short range of the NN interaction, they do not give any noticeable contribution to the source term.

The matrix elements in Eq. (4) were calculated using Ψ_{J_A} and Ψ_{J_B} obtained in the $0\hbar\omega$ space with effective NN interactions from [24]. The effective interaction $v^{\rm eff}_{iA}$ of the removed nucleon with the nucleons in B to be used in Eq. (4) has been taken from Ref. [25] as the M3Y interaction that fits the oscillator matrix elements obtained from NN scattering data in [26]. Unlike in [18], where the calculations were done in the supermultiplet scheme, the present calculations were performed within the M-scheme using the formalism of Ref. [19]. New expressions for two-body matrix elements were derived (see Appendix) which significantly accelerate calculations.

The SFs, ANCs, and the rms radii of the overlap functions obtained in the new STA calculations are shown in Table I. The STA spectroscopic factors $S^{\rm STA}_{lj}$ are compared there with the spectroscopic factors $S^{\rm DE}_{lj}$ obtained by direct evaluation of the overlap integral between the $0\hbar\omega$ shell model wave functions Ψ_P. The ratio $R=(\sum_j S^{\rm STA}_{lj})/(\sum_j S^{\rm DE}_{lj})$ is also plotted in Fig. 1 as a function of difference ΔS of neutron and proton separation energies S_p-S_n or S_n-S_p. The ratios R corresponding to removal of proton and neutron from the same nucleus are joined together by a dashed line. The slope of this line indicates neutron-proton asymmetry of the reduction of the STA spectroscopic factors with respect to the traditional shell model ones. For all $N\neq Z$ nuclei the slopes are rather similar, except for ^{15}N, ^{11}B, and ^{7}Li. They are larger than that predicted in other theoretical approaches, larger than that claimed by transfer experiments but smaller than the ones seen in knockout experiments. The largest asymmetry, about 70%, is obtained for ^{14}O, while for symmetrical $N=Z$ nuclei it is rather small, being 2–5 %. As explained in [18], the ΔS behavior of $S^{\rm STA}/S^{\rm DE}$ originates due to the energy dependence (via κ) of the Green's function in Eq. (1).

From Table I it is seen that in most cases the STA spectroscopic factors are smaller than the corresponding shell model ones. Exceptions are the $j=1/2$ component of the overlap between the wave functions of the 1^+ state in ^{14}N and the wave functions of the $3/2^-$ states in ^{13}O, ^{15}N, and ^{15}O. These overlaps are particularly sensitive to the shape of the tensor part of the source term and to its interference with the contribution from the spin-orbit force. Such a sensitivity can be used in the future to better tune the effective interactions in the STA.

III. ASYMPTOTIC NORMALIZATION COEFFICIENTS: COMPARISON TO EXPERIMENT AND TO CALCULATIONS FROM *ab initio* METHODS

The ANCs, being matrix elements of the virtual decay operator [22], are observable quantities [21]. They can be

TABLE I. The ANC's squared C^2_{lj} in comparison with experimental values $C^2_{\rm exp}$ (in fm^{-1}), the rms radii $\langle r^2\rangle^{1/2}$ (in fm) and the spectroscopic factors $S^{\rm STA}_{lj}$ and $S^{\rm DE}_{lj}$ calculated in the STA and using direct overlap of the shell model wave functions, respectively, for a range of the $\langle A|A-1\rangle$ overlaps in comparison to S_{ab} values from *ab initio* calculations.

A	$A-1$	j	C^2_{lj}	$C^2_{\rm exp}$	$\langle r^2\rangle^{1/2}$	$S^{\rm STA}_{lj}$	$S^{\rm DE}_{lj}$	S_{ab}
^{7}Li($3/2^-$)	^{6}He(0^+)	3/2	5.65	6.15[a]	2.925	0.280	0.693	0.439[b];0.406[c]
^{7}Li($3/2^-$)	^{6}He(2^+)	1/2	3.32		3.007	0.085	0.189	0.137[b]
		3/2	3.95		2.941	0.112	0.255	0.156[b]
		sum	7.27			0.197	0.444	0.293[b]
^{7}Li($3/2^-$)	^{6}Li(1^+)	1/2	1.20		3.183	0.154	0.284	0.242[b];0.230[c]
		3/2	1.79		3.051	0.281	0.586	0.473[b];0.438[c]
		sum	2.99	3.17(53)[d,e]		0.435	0.870	0.715[b];0.668[c]
^{7}Li($3/2^-$)	^{6}Li(3^+)	3/2	4.65	4.24(48)[d,e]	3.028	0.338	0.699	0.476[b];0.435[c]
^{7}Li($3/2^-$)	^{6}Li(0^+)	3/2	2.46	2.91(35)[d,e]	2.911	0.139	0.346	0.221[f];0.203[c]
^{7}Li($1/2^-$)	^{6}He(0^+)	1/2	4.08		3.028	0.198	0.485	
^{7}Li($1/2^-$)	^{6}Li(1^+)	1/2	0.076		3.018	0.018	0.075	0.069[f];0.060[c]
		3/2	3.256		3.101	0.572	1.135	0.854[f];0.759[c]
		sum	3.34			0.590	1.210	0.923[f];0.819[c]
^{7}Be($3/2^-$)	^{6}Li(1^+)	1/2	1.29		3.245	0.163	0.284	0.229[f];0.225[c]
		3/2	1.96		3.122	0.296	0.586	0.480[f];0.438[c]
		sum	3.25	3.13(27)[g]		0.459	0.870	0.709[f];0.663[c]
^{7}Be($3/2^-$)	^{6}Li(3^+)	3/2	5.20		3.068	0.352	0.699	0.500[f];0.457[c]
^{7}Be($3/2^-$)	^{6}Li(0^+)	3/2	2.81		2.945	0.145	0.346	0.221[f];0.210[c]
^{7}Be($3/2^-$)	^{6}Be(0^+)	3/2	4.81		2.916	0.281	0.693	
^{7}Be($3/2^-$)	^{6}Be(2^+)	1/2	2.77		3.003	0.086	0.189	
		3/2	3.30		2.937	0.114	0.255	
		sum	6.07			0.200	0.444	
^{7}Be($1/2^-$)	^{6}Li(1^+)	1/2	0.087		3.077	0.019	0.075	
		3/2	3.564		3.166	0.602	1.135	
		sum	3.66	3.80(35)[g]		0.621	1.210	
^{8}He(0^+)	^{7}He($3/2^-$)	3/2	2.23		3.560	2.57	3.94	
^{8}Li(2^+)	^{7}He($3/2^-$)	1/2	3.00		2.915	0.065	0.146	
		3/2	13.3		2.871	0.328	0.785	
		sum	16.3			0.393	0.931	0.58[h]
^{8}Li(2^+)	^{7}He($5/2^-$)	1/2	2.90		2.890	0.032	0.060	
		3/2	5.39		2.848	0.064	0.139	
		sum	8.29			0.096	0.199	0.17[h]
^{8}Li(2^+)	^{7}Li($3/2^-$)	1/2	0.027		3.738	0.044	0.064	0.082[b]
		3/2	0.337		3.627	0.616	1.079	0.884[b]
		sum	0.364	0.432(44)[d]		0.660	1.143	0.966[b]
^{8}Li(2^+)	^{7}Li($1/2^-$)	3/2	0.120		3.496	0.157	0.281	0.263[b]
^{8}Li(1^+)	^{7}Li($3/2^-$)	1/2	0.012		4.153	0.054	0.100	
		3/2	0.054		4.072	0.268	0.417	
		sum	0.066	0.083(15)[d]		0.322	0.517	
^{8}Be(0^+)	^{7}Li($3/2^-$)	3/2	90.3		2.794	0.668	1.721	
^{8}Be(0^+)	^{7}Be($3/2^-$)	3/2	77.2		2.779	0.653	1.721	
^{8}B(2^+)	^{7}Be($3/2^-$)	1/2	0.033		4.537	0.053	0.064	0.082[b]
		3/2	0.418		4.399	0.742	1.079	0.884[b]
		sum	0.441	0.452(81)[d]		0.795	1.143	0.966[b]
^{8}B(2^+)	^{7}Be($1/2^-$)	3/2	0.099		3.951	0.183	0.281	0.263[b]
^{8}B(2^+)	^{7}B($3/2^-$)	1/2	2.51		2.911	0.066	0.146	
		3/2	11.1		2.868	0.332	0.785	
		sum	13.6			0.398	0.931	

TABLE I. (*Continued.*)

A	$A-1$	j	C^2_{lj}	$C^2_{\rm exp}$	$\langle r^2\rangle^{1/2}$	$S^{\rm STA}_{lj}$	$S^{\rm DE}_{lj}$	S_{ab}
^{9}Li($3/2^-$)	^{8}He(0^+)	3/2	22.2		2.819	0.384	0.935	0.573[b]
^{9}Li($3/2^-$)	^{8}Li(2^+)	1/2	0.035		3.343	0.016	0.029	0.109[b]
		3/2	1.159		3.279	0.584	1.016	0.993[b]
		sum	1.184	1.33(33)[d]		0.600	1.045	1.104[b]
^{9}Li($3/2^-$)	^{8}Li(1^+)	1/2	0.127		3.301	0.035	0.060	0.008[b]
		3/2	0.876		3.184	0.284	0.509	0.460[b]
		sum	1.003			0.319	0.569	0.468[b]
^{9}Li($3/2^-$)	^{8}Li(3^+)	3/2	4.51		3.127	0.850	1.512	
^{9}Li($1/2^-$)	^{8}Li(2^+)	3/2	0.109		3.997	0.324	0.426	
^{9}Be($3/2^-$)	^{8}Li(2^+)	1/2	8.07		2.849	0.056	0.126	0.162[b]
		3/2	53.0		2.790	0.401	1.000	0.607[b]
		sum	61.1			0.457	1.126	0.769[b]
^{9}Be($3/2^-$)	^{8}Li(1^+)	1/2	19.8		2.826	0.107	0.236	0.226[b]
		3/2	17.4		2.765	0.109	0.267	0.202[b]
		sum	37.2			0.216	0.503	0.428[b]
^{9}Be($3/2^-$)	^{8}Be(0^+)	3/2	0.175	0.27(9)[d]	3.776	0.416	0.627	0.581[b]
^{9}Be($3/2^-$)	^{8}Be(2^+)	1/2	0.081		3.341	0.027	0.042	0.040[b]
		3/2	1.26		3.246	0.463	0.817	0.583[b]
		sum	1.34	2.0(11)[d]		0.490	0.859	0.623[b]
^{9}B($3/2^-$)	^{8}B(2^+)	1/2	6.97		2.833	0.055	0.126	0.109[b]
		3/2	45.5		2.774	0.391	1.000	0.993[b]
		sum	52.5			0.446	1.126	1.104[b]
^{9}C($3/2^-$)	^{8}B(2^+)	1/2	0.035		3.678	0.020	0.029	
		3/2	1.055		3.597	0.693	1.016	
		sum	1.080	1.11(26)[d]		0.713	1.045	
^{9}C($3/2^-$)	^{8}C(0^+)	3/2	17.7		2.822	0.396	0.935	
^{10}Be(0^+)	^{9}Li($3/2^-$)	3/2	179.6		2.732	0.821	1.93	1.137[b]
^{10}Be(0^+)	^{9}Li($1/2^-$)	1/2	54.4		2.730	0.139	0.276	0.435[b]
^{10}Be(0^+)	^{9}Be($3/2^-$)	3/2	9.12		3.042	1.515	2.672	2.084[b];2.36[i]
^{10}B(3^+)	^{9}Be($3/2^-$)	3/2	3.53	5.12(51)[d];3.53(52)[j]	2.942	0.315	0.665	
^{10}B(3^+)	^{9}B($3/2^-$)	3/2	2.73	1.93(29)[d];2.59(48)[j]	2.897	0.302	0.665	
^{10}B(3^+)	^{9}B($5/2^-$)	1/2	0.869		2.919	0.039	0.068	
		3/2	5.71		2.862	0.295	0.638	
		sum	6.58	2.15(29)[d]		0.334	0.706	
^{10}B(1^+_1)	^{9}Be($3/2^-$)	1/2	2.46		3.073	0.240	0.432	
		3/2	2.82		3.081	0.273	0.506	
		sum	5.28	6.6(2.5)[d]		0.513	0.938	
^{10}B(0^+_1)	^{9}Be($3/2^-$)	3/2	5.53	6.2(24)	3.113	0.802	1.34	
^{10}B(1^+_2)	^{9}Be($3/2^-$)	1/2	0.255		3.161	0.042	0.081	
		3/2	0.737		3.061	0.142	0.252	
		sum	0.992	1.28(35)[d]		0.184	0.333	
^{10}C(0^+)	^{9}B($3/2^-$)	3/2	10.2		3.159	1.62	2.67	2.084[b]
^{10}C(0^+)	^{9}C($3/2^-$)	3/2	154		2.720	0.808	1.93	1.137[b];1.52[i]
^{11}B($3/2^-_1$)	^{10}Be(0^+)	3/2	8.56		2.748	0.232	0.465	
^{11}B($3/2^-_1$)	^{10}B(3^+)	3/2	13.7	31.6(18)[d]	2.822	0.635	1.120	
^{11}B($3/2^-_1$)	^{10}B(1^+)	1/2	1.93		2.825	0.069	0.106	
		3/2	2.59		2.791	0.103	0.187	
		sum	4.52	14.9(18)[d]		0.172	0.293	
^{11}C($3/2^-_1$)	^{10}B(3^+)	3/2	17.63	29(5)[d]	2.872	0.672	1.120	
^{11}C($3/2^-$)	^{10}C(0^+)	3/2	6.53		2.723	0.226	0.465	
^{12}B(1^+)	^{11}B($3/2^-$)	1/2	0.924		3.291	0.670	0.783	
		3/2	0.209		3.362	0.143	0.205	

TABLE I. (*Continued.*)

A	$A-1$	j	C^2_{lj}	$C^2_{\rm exp}$	$\langle r^2\rangle^{1/2}$	$S^{\rm STA}_{lj}$	$S^{\rm DE}_{lj}$	S_{ab}
		sum	1.133	1.20(26)[d]		0.813	0.988	
^{12}C(0^+)	^{11}B($3/2^-_1$)	3/2	199	223(31)[d]	2.688	1.54	2.855	
^{12}C(0^+)	^{11}B($1/2^-$)	1/2	104		2.695	0.484	0.832	
^{12}C(0^+)	^{11}B($3/2^-_2$)	3/2	112		2.663	0.332	0.612	
^{12}C(0^+)	^{11}C($3/2^-_1$)	3/2	150.		2.663	1.485	2.855	
^{12}C(0^+)	^{11}C($1/2^-$)	1/2	77.9		2.674	0.476	0.832	
^{12}C(0^+)	^{11}C($3/2^-_2$)	3/2	82.9		2.648	0.327	0.612	
^{12}C(2^+)	^{11}B($3/2^-$)	1/2	22.0	15.8(35)[d]	2.788	0.400	0.598	
		3/2	0.264		2.538	0.008	0.013	
^{12}N(1^+)	^{11}C($3/2^-$)	1/2	1.376		3.673	0.755	0.783	
		3/2	0.314		3.745	0.164	0.205	
		sum	1.690	1.68(30)[d]		0.919	0.988	
^{13}B($3/2^-$)	^{12}B(1^+)	1/2	1.74		3.140	0.558	0.595	
		3/2	0.31		3.132	0.109	0.126	
		sum	2.05			0.667	0.721	
^{13}C($1/2^-$)	^{12}B(1^+)	1/2	2.42		2.733	0.013	0.014	
		3/2	106		2.609	0.679	1.197	
		sum	108			0.692	1.211	
^{13}C($1/2^-$)	^{12}C(0^+)	1/2	1.50	2.46(31)[d]	3.067	0.532	0.633	
^{13}C($1/2^-$)	^{12}C(2^+)	3/2	7.89	10.4(12)[d]	2.843	0.661	1.116	
^{13}N($1/2^-$)	^{12}C(0^+)	1/2	1.90	3.26(25)[d];2.67(29)[k]	3.270	0.586	0.633	
^{13}N($1/2^-$)	^{12}N(1^+)	1/2	1.81		2.715	0.012	0.014	
		3/2	77.3		2.590	0.668	1.197	
		sum	78.6			0.693	1.211	
^{13}O($3/2^-$)	^{12}N(1^+)	1/2	2.60		3.382	0.635	0.595	
		3/2	0.47		3.363	0.120	0.126	
		sum	3.07	2.53(30)[d];3.9(15)[l]		0.755	0.721	
^{14}C(0^+)	^{13}B($3/2^-$)	3/2	803		2.673	2.087	4.07	
^{14}C(0^+)	^{13}C($1/2^-$)	1/2	16.70		2.970	1.573	1.87	
^{14}N(1^+_1)	^{13}C($1/2^-$)	1/2	14.3		2.900	0.541	0.705	
		3/2	0.22		3.319	0.004	0.013	
		sum	14.5	17.9(30)[d]		0.545	0.718	
^{14}N(0^+)	^{13}C($1/2^-$)	1/2	11.9	11.7(37)[d]	3.056	0.831	0.933	
^{14}N(1^+_2)	^{13}C($1/2^-$)	1/2	1.35		3.263	0.152	0.130	
		3/2	0.65		3.122	0.094	0.144	
		sum	2.00			0.246	0.274	
^{14}N(2^+)	^{13}C($1/2^-$)	3/2	0.091	0.26(4)[d]	3.718	0.047	0.051	
^{14}N(1^+_1)	^{13}N($1/2^-$)	1/2	9.88		2.839	0.517	0.705	
		3/2	0.15		3.268	0.003	0.012	
		sum	10.0	15.4(19)[d]		0.520	0.717	
^{14}N(1^+_1)	^{13}N($3/2^-$)	1/2	2.68		2.768	0.060	0.129	
		3/2	0.59		2.618	0.019	0.027	
		sum	3.27			0.079	0.156	
^{14}O(0^+)	^{13}N($1/2^-$)	1/2	25.0	28.8(45)[d]	3.080	1.69	1.87	1.58[m]
^{14}O(0^+)	^{13}N($3/2^-$)	3/2	60.2		2.915	1.55	2.33	1.90[m]
^{14}O(0^+)	^{13}O($3/2^-$)	3/2	594		2.658	2.14	4.07	3.17[m]
^{15}N($1/2^-$)	^{14}C(0^+)	1/2	43.2		2.853	0.754	0.996	
^{15}N($1/2^-$)	^{14}N(1^+)	1/2	26.8		2.896	1.123	1.36	
		3/2	1.8		2.769	0.108	0.12	
		sum	28.6			1.231	1.48	
^{15}N($3/2^-$)	^{14}C(0^+)	3/2	0.169		3.115	0.021	0.038	
^{15}N($3/2^-$)	^{14}N(1^+)	1/2	0.317		3.441	0.085	0.061	

TABLE I. (*Continued.*)

A	$A-1$	j	C^2_{lj}	$C^2_{\rm exp}$	$\langle r^2\rangle^{1/2}$	$S^{\rm STA}_{lj}$	$S^{\rm DE}_{lj}$	S_{ab}
		3/2	0.0002		3.064	0.0001	0.0002	
		sum	0.317			0.085	0.061	
^{15}O(1/2$^-$)	^{14}N(1$^+$)	1/2	41.2		2.967	1.18	1.36	
		3/2	2.7		2.832	0.11	0.12	
		sum	43.9	60(17)[d]		1.29	1.48	
^{15}O(1/2$^-$)	^{14}O(0$^+$)	1/2	29.5		2.809	0.726	0.996	
^{15}O(3/2$^-$)	^{14}N(1$^+$)	1/2	0.490		3.767	0.098	0.061	
		3/2	0.0002		3.330	0.0001	0.0002	
		sum	0.490	0.46(11)[d]		0.098	0.061	
^{15}O(3/2$^-$)	^{14}O(0$^+$)	3/2	0.117		2.986	0.018	0.038	
^{16}O(0$^+$)	^{15}N(1/2$^-$)	1/2	197	175(29)	2.919	1.38	2.13	1.74[m];1.70[n]
^{16}O(0$^+$)	^{15}N(3/2$^-$)	3/2	1251		2.821	2.42	4.27	3.45[m];3.24[n]
^{16}O(0$^+$)	^{15}O(1/2$^-$)	1/2	125		2.876	1.31	2.13	1.73[m]
^{16}O(0$^+$)	^{15}O(3/2$^-$)	3/2	780		2.797	2.34	4.27	

[a]From Ref. [27].
[b]VMC calculations fron Ref. [28].
[c]GFMC calculations from Ref. [11].
[d]From compilation of [18]. Where several $C^2_{\rm exp}$ are available an average is given that covers all possible experimental values.
[e]These are the values obtained from the ^{7}Li$(d,t)^6$Li measured in [29] at $E_d = 18$ MeV with high precision including the area of small angles. Higher values are also available in [29] but they were obtained from the analysis of less accurate data available elsewhere.
[f]VMC calculations from Ref. [11].
[g]From ^{6}Li(^{3}He,d)^{7}Be reaction [30].
[h]VMC calculations from Ref. [31].
[i]NCSM calculations from Ref. [12].
[j]From ^{10}B(d,^{3}He) and ^{10}B(d,t) reactions [32].
[k]From transfer reaction ^{12}C(^{7}Li,^{6}He)^{13}N [33].
[l]From ^{12}N$(d,n)^{13}$O reaction [34].
[m]SCGF calculations from Ref. [10].
[n]CCM calculations from Ref. [14].

deduced directly from the peripheral reactions cross sections. Transfer reactions are most frequently used for these purposes.

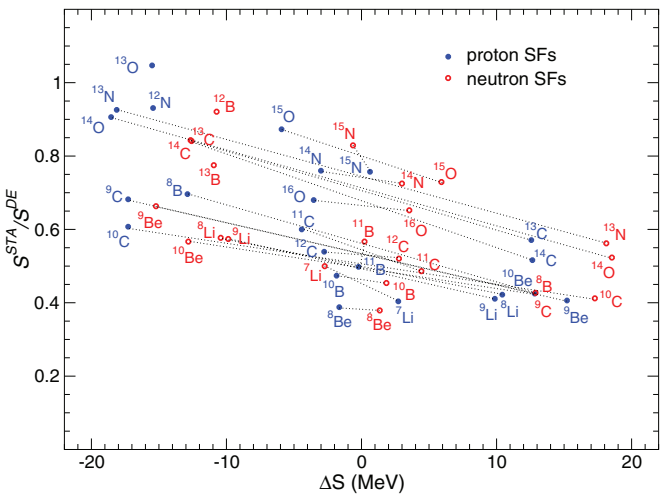

FIG. 1. (Color online) The ratio $S^{\rm STA}/S^{\rm DE}$ of the spectroscopic factors obtained in STA and from direct evaluation of the shell model wave functions as a function of ΔS, which is $S_p - S_n$ or $S_n - S_p$ for proton or neutron removal, respectively.

The compilation of experimental ANCs squared $C^2_{\rm exp}$ for $0p$-shell nuclei is available in Ref. [18] with a detailed discussion of their uncertainties and further referencing. The $C^2_{\rm exp}$ values with the errors that cover all possible experimental values, summarized in [18], are shown in Table I. A few recent $C^2_{\rm exp}$ values are added there: the previously unknown ANC for ^{7}Be$\rightarrow^6$Li$+p$ [30] and the new values for the ^{10}B$\rightarrow^9$Be$+p$, ^{10}B$\rightarrow^9$B$+n$ [32], ^{13}N$\rightarrow^{12}$C$+p$ [33], and ^{13}O$\rightarrow^{12}$N$+p$ [34] vertices. The new proton ANC for ^{13}O and new neutron ANC for ^{10}B agree within the error bars with earlier determinations in Refs. [29,35] while the new proton ANCs for ^{10}B and ^{13}N are smaller than the values deduced previously in Refs. [36,37]. The ratio of $C^2_{\rm exp} = \sum_j C^2_{\rm exp}(lj)$ to the STA values $C^2_{\rm STA} = \sum_j C^2_{lj}$ are shown in Fig. 2. In many cases the STA reproduces the experimental values within the error bars, however, these bars are often too large due to different ANC values for the same vertex deduced from different reactions. In those cases where the STA clearly underpredict the ANCs, such as ^{13}C, ^{13}N, ^{11}B, these ANCs are strongly influenced by the interference of different $|[f]LST\rangle$ components and, to a lesser extent, by non-central components of $v^{\rm eff}$. Further tuning of effective shell model Hamiltonians H_{PP} determining the nuclear spectra and the interaction $v^{\rm eff}$ of removed nucleon with nucleons in B, may fix this problem.

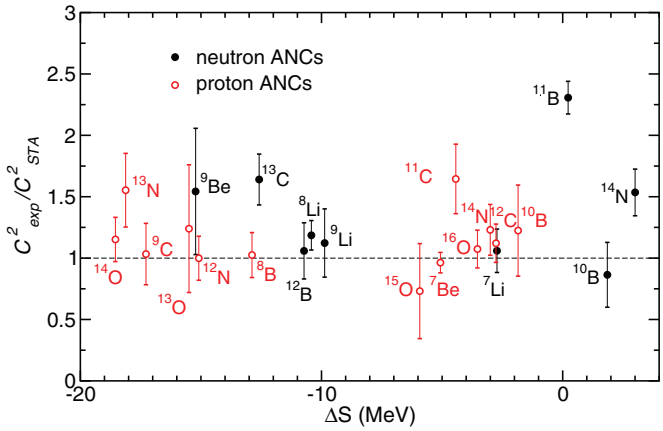

FIG. 2. (Color online) The ratio of experimental to theoretical ANC's squared for neutrons (filled circles) and protons (open circles), calculated in the STA, for a range of the ground state of 0p-shell nuclei as a function of ΔS taken as $S_p - S_n$ or $S_n - S_p$ for proton or neutron removal, respectively.

Ab initio approaches rarely give ANCs. To provide ANCs these methods should be able to get converged $I_{lj}(r)$ at large r with correct decay constant. This is very difficult to achieve because such calculations require large model spaces to which the total binding energies are not sensitive. For $A \leqslant 7$, the *ab initio* GFMC calculations for $I_{lj}(r)$ are available up to $r \sim 6$ fm where the asymptotic behavior is mostly achieved and the nucleon separation energies are reproduced so that the ANCs can be determined with a reasonable accuracy [11]. Another *ab initio* method, VMC, does not reproduce separation energies correctly and it does not predict any definite behavior of $I_{lj}(r)$ at large r [28]. The ANCs can be recovered in VMC only from potential model calculations that fit $I_{lj}(r)$ inside the nuclear region [13] but such ANCs are not very accurate since small changes in $I_{lj}(r)$ within statistical VMC errors at small r can give noticeable uncertainties at large r. The VMC can be used, however, to generate ANCs in the source term calculations as is done in Ref. [38]. Otherwise, to guarantee the correct asymptotic behavior of $I_{lj}(r)$, R-matrix ideas should be used. At present, only one example of the R-matrix calculations of ANCs that uses *ab initio* wave function of the core is known: this is the ANC calculation for ^{8}B obtained within the NCSM combined with the R-matrix approach [39]. Other microscopic cluster model R-matrix calculations, for example in [40], use simplified models of clusters' internal wave functions and overpredict ANCs with the NN potentials well adapted for such calculations [41].

The ANCs obtained within the shell model (SM) STA are compared to the GFMC [11] and VMC-STA [38] calculations in Table II as well as to the $C^2_{\rm exp}$ values. The SM-STA C^2 values are always smaller than the results from other approaches. For weakly bound nuclei such as ^{8}Li, ^{8}B, ^{9}Li, and ^{9}C the difference between the SM-STA, VMC-STA, and NCSM values of C^2 does not exceed 25% [except for $^9\mathrm{Li}(3/2^-) \rightarrow {}^8\mathrm{Li}(1^+) + n$]. All these C^2 agree with $C^2_{\rm exp}$ within the error bars. For all other cases, the SM-STA C^2 values are 2–3 times smaller than those predicted by the VMC-STA or GFMC. The most obvious reason for that could lie in the absence of the cluster degrees of freedom in the SM-STA. However, the experimental $C^2_{\rm exp}$ values for ^{7}Li and ^{7}Be favour the SM-STA values. It is also possible that the experimental cross sections used to deduce $C^2_{\rm exp}$ for these nuclei are strongly influenced by the cluster degrees of freedom which are not explicitly taken into account in the analysis of transfer reaction data.

TABLE II. The ANC's squared $C^2 = \sum_j C^2_{lj}$ (in fm^{-1}), for a range of the $\langle A|A-1\rangle$ overlaps calculated within the shell model (SM) STA and within *ab initio* VMC-STA [38], GFMC [11], and NCSM [39] approaches in comparison with the experimental $C^2_{\rm exp}$ values. See Table I for references and discussion of $C^2_{\rm exp}$.

A	$A-1$	SM-STA	VMC-STA	GFMC	NSCM	$C^2_{\rm exp}$
^{7}Li($3/2^-$)	^{6}He(0^+)	5.65	13.5	12.4		6.15
^{7}Li($3/2^-$)	^{6}Li(1^+)	2.99	6.29	8.24		3.17(53)
^{7}Li($3/2^-$)	^{6}Li(3^+)	4.65		12.3		4.24(48)
^{7}Li($3/2^-$)	^{6}Li(0^+)	2.46		5.71-6.05		2.91(35)
^{7}Li($1/2^-$)	^{6}He(0^+)	4.08	12.2			
^{7}Li($1/2^-$)	^{6}Li(1^+)	3.34	6.75	8.47		
^{7}Be($3/2^-$)	^{6}Li(1^+)	3.25	8.12	7.73		3.13(27)
^{7}Be($3/2^-$)	^{6}Li(3^+)	5.20		12.2		
^{7}Be($3/2^-$)	^{6}Li(0^+)	2.81		6.66		
^{7}Be($1/2^-$)	^{6}Li(1^+)	3.66	7.02			3.80(35)
^{8}Li(2^+)	^{7}Li($3/2^-$)	0.364	0.429			0.432(44)
^{8}Li(1^+)	^{7}Li($3/2^-$)	0.066	0.087			0.083(15)
^{8}B(2^+)	^{7}Be($3/2^-$)	0.441	0.538		0.509	0.455(77)
^{9}Li($3/2^-$)	^{8}He(0^+)	22.2	36.0			
^{9}Li($3/2^-$)	^{8}Li(2^+)	1.184	1.39			1.33(33)
^{9}Li($3/2^-$)	^{8}Li(1^+)	1.003	0.498			
^{9}Be($3/2^-$)	^{8}Li(2^+)	61.1	116.			
^{9}Be($3/2^-$)	^{8}Li(1^+)	37.2	81.6			
^{9}C($3/2^-$)	^{8}B(2^+)	1.080	1.36			1.11(26)

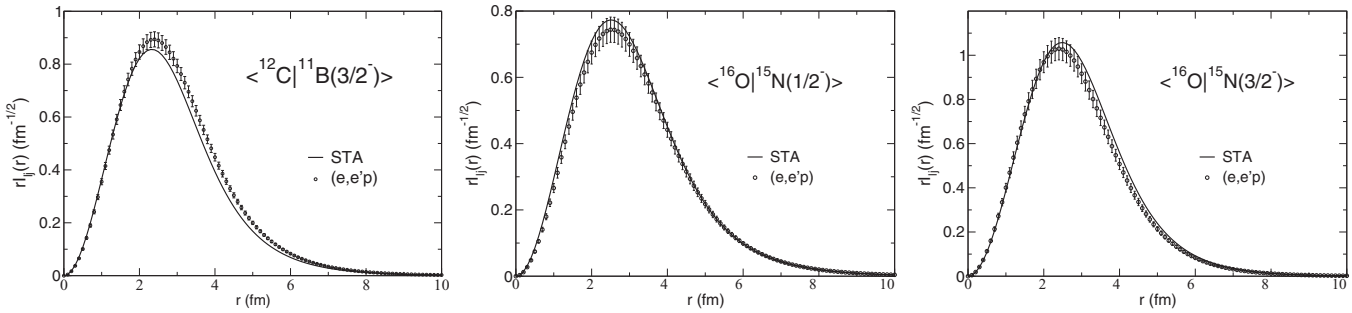

FIG. 3. The $\langle {}^{12}\mathrm{C}|{}^{11}\mathrm{B}(3/2^-_1)\rangle$, $\langle {}^{16}\mathrm{O}|{}^{15}\mathrm{N}(1/2^-_1)\rangle$, and $\langle {}^{16}\mathrm{O}|{}^{15}\mathrm{N}(3/2^-_1)\rangle$ overlap functions calculated in the STA in comparison to those that fit the $(e, e'p)$ cross sections.

IV. SPECTROSCOPIC FACTORS: EXPERIMENTAL STATUS AND COMPARISON TO *ab initio* APPROACHES

Although, strictly speaking, the spectroscopic factors are not observables since they are not invariant amplitudes of any description [21], in reality they can be calculated from the overlap integrals that best fit experimental cross sections. The $(e, e'p)$ reactions are best suited for this purpose as their momentum distributions are related to Fourier transforms of $I_{lj}(r)$ distorted by the final state interactions. The overlaps $I_{lj}(r)$ can be always modelled by two-body potential well calculations with the parameters fitted to reproduce the $(e, e'p)$ cross sections. For $0p$-shell nuclei such phenomenological overlaps are available for two nuclei: ^{12}C and ^{16}O [2]. Their norms can be considered as experimental values S_{exp} of spectroscopic factors. For ^{16}O, S_{exp} is equal to 1.27(13) and 2.25(22) for the final $^{15}\mathrm{N}(1/2^-_1)$ and $^{15}\mathrm{N}(3/2^-_1)$ states, respectively. For ^{12}C, S_{exp} is 1.72(11), 0.26(2) and 0.20(2) for the final states $^{11}\mathrm{B}(3/2^-_1)$, $^{11}\mathrm{B}(1/2^-_1)$, and $^{11}\mathrm{B}(3/2^-_2)$. The overlaps $\langle {}^{16}\mathrm{O}|{}^{15}\mathrm{N}(1/2^-_1)\rangle$, $\langle {}^{16}\mathrm{O}|{}^{15}\mathrm{N}(3/2^-_1)\rangle$, and $\langle {}^{12}\mathrm{C}|{}^{11}\mathrm{B}(3/2^-_1)\rangle$ obtained in the STA are close to those obtained phenomenologically (see Fig. 3) and their are SFs close to S_{exp}. The SFs for $\langle {}^{12}\mathrm{C}|{}^{11}\mathrm{B}(1/2^-_1)\rangle$ and $\langle {}^{12}\mathrm{C}|{}^{11}\mathrm{B}(3/2^-_2)\rangle$ are about 70% larger than the ones from $(e, e'p)$ but this is related to the interference between the shell model configurations rather than uncertainties in v^{eff}_{iA}.

The situation with $^7\mathrm{Li}(e, e'p)^6\mathrm{He}$ is less clear. On the one hand, momentum distribution of this reaction calculated with the VMC overlap function with $S_{\mathrm{VMC}} = 0.44$ reproduce the observed ones [42]. However, the inclusive $^9\mathrm{Be}(^7\mathrm{Li},^6\mathrm{He})$ proton knockout cross section, calculated in the eikonal reaction model using the same VMC overlap function [13], is twice the experimental one. Renormalization of the VMC overlap to fit the knockout data would give the spectroscopic factor of 0.22, which is not far away from the STA prediction of 0.28. The need of large renormalization of the calculated knockout cross sections can be explained by the lack of appropriate treatment of the weak binding in ^{6}He. However, the weak binding in ^{6}He has not been taken into account in the final state of the $(e, e'p)$ reaction as well, which could influence the interpretation of this reaction.

The proton knockout cross sections for other light nuclei calculated in the eikonal model with VMC overlaps also need to be renormalized by a factor $\mathcal{R}$ shown in Table III together with the product $\mathcal{R}S_{\mathrm{VMC}}$. The knockout cross sections are mostly determined by the product of spectroscopic factor and the rms radius of the overlap function [13]. Therefore, to estimate a possible outcome of the eikonal calculations with the STA overlap the ratio $\mathcal{R}_r = (\langle r^2\rangle_{\mathrm{STA}}/\langle r^2\rangle_{\mathrm{VMC}})^{1/2}$ times S_{STA} is compared to $\mathcal{R}S_{\mathrm{VMC}}$ in Table III. This comparison suggests that the eikonal model with the STA overlap would reproduce the experimental knockout cross sections for ^{7}Li and ^{10}C but would give smaller cross sections for proton knockout from ^{9}Li, ^{9}Be and for neutron knockout from ^{10}Be, while for proton knockout from ^{10}Be these cross sections will be larger than the experimental ones.

Apart from nucleon knockout, the nucleon transfer reactions are always quoted as a good source of experimental spectroscopic factors. However, the transfer cross sections are often sensitive only to the peripheral part of $I_{lj}(r)$ which makes them a good source of ANCs rather than SFs. In the previous publication [18], the STA spectroscopic factors were compared to the renormalization factors obtained from (d, p) and (p, d) reactions analyzed in Ref. [3] within the adiabatic Johnson-Tandy theory [43] using single-particle wave functions from Hartree-Fock calculations. However, recently it became clear that the correction for nonlocality by a simple modification of the deuteron distortion waves in the nuclear interior, made in [3], has been not justified [44]. Moreover, it has been shown recently that proper treatment of non-locality of nucleon optical potentials may significantly change the interpretation of the (d, p) and (p, d) data [44] both

TABLE III. Renormalization factor $\mathcal{R}$ that lowers the eikonal model knockout cross sections down to measured ones [13], the VMC spectroscopic factor renormalized by $\mathcal{R}$ in comparison with the STA spectroscopic factor S_{STA} and the STA spectroscopic factor renormalized by $\mathcal{R}_r = (\langle r^2\rangle_{\mathrm{STA}}/\langle r^2\rangle_{\mathrm{VMC}})^{1/2}$.

A	$A-1$	$\mathcal{R}$	$\mathcal{R}S_{\mathrm{VMC}}$	S_{STA}	$\mathcal{R}_r S_{\mathrm{STA}}$
^{7}Li	^{6}He	0.5	0.22	0.28	0.25
	$^6\mathrm{Li}(1^+)$		0.42	0.44	0.41
	$^6\mathrm{Li}(0^+)$		0.13	0.14	0.13
^{9}Li	$^8\mathrm{Li}(2^+)$	0.71	0.78	0.60	0.57
	$^8\mathrm{Li}(1^+)$		0.33	0.32	0.31
^{9}C	$^8\mathrm{B}(2^+)$	0.87	0.96	0.71	0.73
^{10}Be	$^9\mathrm{Li}(3/2^-)$	0.52	0.54	0.82	0.79
	$^9\mathrm{Li}(1/2^-)$		0.22	0.14	0.13
	$^9\mathrm{Be}(3/2^-)$	0.97	1.88	1.52	1.49
^{10}C	$^9\mathrm{C}(3/2^-)$	0.74	0.74	0.81	0.77

for absolute and relative spectroscopic factors [45]. Therefore, no comparison to renormalization factors obtained in transfer reactions and called spectroscopic factors is done in present work. A better understanding of transfer reaction theory is needed for these purposes.

V. CONCLUSIONS

In the present paper, nearly 30 new ANCs, spectroscopic factors and rms radii of overlap functions for $0p$-shell nuclei are tabulated while the results from previous calculations [18] are updated. These quantities have been calculated within the STA in which the missing subspaces are taken into account via phenomenological effective interactions of the removed nucleon with the nucleons from residual nucleus. These calculations confirm the reduction of spectroscopic factors with respect to those calculated using the standard approach that involves overlapping shell model wave functions defined in a restricted model space. Significant neutron-proton asymmetry in spectroscopic factor reduction for proton and neutron removal is also predicted for $N \neq Z$ nuclei.

The STA spectroscopic factors are smaller than those calculated in *ab initio* approaches such as VMC, GFMC, SCGFM, and CCM. The ANCs from STA are also smaller than those available from VMC, GFMC, and NCSM calculations. Comparison with experimental data suggests that STA gives reasonable predictions of those quantities for many cases. However, it should be kept in mind that experimental values are often strongly influenced by uncertainties of the reaction model and that sometimes different values are obtained for the same quantities from different reactions. This urges further development of reaction theory aimed to extract properties of the overlap functions from nucleon removal reactions.

ACKNOWLEDGMENTS

I am grateful to P. Descouvemont for providing me with the code generating the $|LSTJ\rangle$ states in the M-scheme. The support from the UK STFC ST/J000051/1 grant is also gratefully acknowledged.

APPENDIX

The expressions for the source term can be found in Secs. II and III of Ref. [18] while the analytical expressions for two-body matrix elements making up the source term are given in the Appendix of Ref. [18]. In the present work, a simplification of these expressions has been found that significantly accelerates numerical calculations. The new expressions will be particularly important for future applications of STA for heavy nuclei and for large orbital momenta of removed nucleons.

According to [18], the two-body matrix elements in momentum space, needed for the source term calculations, are

$$U^{\alpha_1\alpha_2\alpha_3}_{ljm_j\tau}(q) = \sum_{m\sigma}\left(lm\frac{1}{2}\sigma|jm_j\right) i^l \int d\hat{\boldsymbol{q}}\, Y^*_{lm}(\hat{\boldsymbol{q}})\langle\phi_{\alpha_1}(\boldsymbol{r}_1)e^{-\gamma \boldsymbol{q}\boldsymbol{r}_2}\chi_{\frac{1}{2}\sigma}(A)\chi_{\frac{1}{2}\tau}(A)|\hat{V}(\boldsymbol{r}_{12})|\phi_{\alpha_2}(\boldsymbol{r}_1)\phi_{\alpha_3}(\boldsymbol{r}_2)\rangle, \tag{A1}$$

where $\phi_\alpha(\boldsymbol{r})$ is the single-particle oscillator wave function with the quantum numbers $\alpha = \{n, l, j, m_j, \tau\}$ representing the total number of oscillator quanta, orbital momentum, angular momentum, its projection, and the projection of isospin of the nucleon. Also, $\chi_{\frac{1}{2}\sigma(\tau)}(A)$ is the spin (isospin) function of the removed nucleon and

$$\gamma = \frac{2A-1}{2A}\sqrt{\frac{A}{A-1}}. \tag{A2}$$

The two-body NN potential in Eq. (A1) has the contributions from the central (c), spin-orbit (so), and tensor (t) parts:

$$\hat{V}(\boldsymbol{r}_{12}) = \sum_{S,T=0,1} V^{\rm c}_{ST}(r_{12})\hat{P}_S(1,2)\hat{P}_T(1,2) + \sum_{T=0,1}((\boldsymbol{L}\cdot\boldsymbol{S})V^{\rm so}_T(r_{12}) + \hat{S}_{12}\,V^{\rm t}_T(r_{12}))\hat{P}_T(1,2), \tag{A3}$$

where $\hat{P}_S$ ($\hat{P}_T$) is the projection operator into two-nucleon state with spin S (isospin T), $\boldsymbol{L}$ and $\boldsymbol{S}$ are the operator of the orbital momentum and spin of the NN pair, respectively, and $\hat{S}_{12} = 3(\boldsymbol{\sigma}_1\boldsymbol{r}_{12})(\boldsymbol{\sigma}_2\boldsymbol{r}_{12})/r^2_{12} - (\boldsymbol{\sigma}_2\boldsymbol{\sigma}_1)$, $\boldsymbol{r}_{12} = \boldsymbol{r}_1 - \boldsymbol{r}_2$.

The new expressions for $U^{\alpha_1\alpha_2\alpha_3}_{ljm_j\tau}(q)$ are given below. For the central interaction in the ST channel

$$\begin{aligned}
U^{\alpha_1\alpha_2\alpha_3}_{ljm_j\tau}(q) = {} & \sum_{JM_JM_T}(j_2m_2j_3m_3|JM_J)(j_1m_1jm_j|JM_J)\left(\tfrac{1}{2}\tau_1\tfrac{1}{2}\tau|TM_T\right)\left(\tfrac{1}{2}\tau_2\tfrac{1}{2}\tau_3|TM_T\right)\ \hat{l}\hat{j}\hat{j}_1\hat{j}_2\hat{j}_3 \\
& \times\sum_{LS}(-)^{l+L}\,\hat{L}^2\hat{S}^2\begin{Bmatrix} l_1 & \frac{1}{2} & j_1 \\ l & \frac{1}{2} & j \\ L & S & J\end{Bmatrix}\begin{Bmatrix} l_2 & \frac{1}{2} & j_2 \\ l_3 & \frac{1}{2} & j_3 \\ L & S & J\end{Bmatrix}\sum_{NN'L'\Lambda'n'l'}\langle n'l'N'\Lambda' : l|2:1|NL'n_3l_3 : l\rangle\phi_{n'l'}\left(\frac{\gamma q}{\sqrt{3}}\right) \\
& \times(-)^{n'+(l'+\Lambda'+l)/2+L'+1}\,\hat{l}'\hat{L}'(l'0l|\Lambda'0)W(l_2l_3l_1l;LL')\left[\sum_\nu\phi_{\nu0}(0)\langle\nu0NL' : L'|1:1|n_1l_1n_2l_2 : L'\rangle\right] \\
& \times\pi^{3/2}\int_0^\infty ds s^2 V^{(c)}_{ST}\left(\sqrt{\tfrac{3}{2}}s\right) j_{\Lambda'}\left(\sqrt{\tfrac{2}{3}}\gamma sq\right)\phi_{N'\Lambda'}(s),
\end{aligned} \tag{A4}$$

where $\hat{i} = \sqrt{2i+1}$, $(j_1 m_1 j_2 m_2 | J M)$ is the Clebsch-Gordan coefficient, the quantities in the figure brackets are the $9j$ symbols, W are the Racah coefficients, $\langle n_1 l_1 n_2 l_2' : l | \mu_2 : \mu_1 | n_1' l_1' n_2' l_2' \rangle$ are the Talmi-Moshinsky coefficients for particles with masses μ_1 and μ_2 [46], and j is the spherical Bessel function. Also, $\phi_{\nu 0}(0)$ and $\phi_{n'l'}(\gamma q/\sqrt{3})$ are the single-particle oscillator functions in the coordinate and momentum space, respectively [18].

For the spin-orbit ($i = \mathrm{so}$) and tensor ($i = \mathrm{t}$) interactions the $U^{\alpha_1\alpha_2\alpha_3}_{ljm_j\tau}(q)$ in the channel with isospin T is

$$
\begin{aligned}
U^{\alpha_1\alpha_2\alpha_3}_{ljm_j\tau}(q) = & \sum_{JM_JM_T} (j_2 m_2 j_3 m_3 | J M_J)(j_1 m_1 j m_j | J M_J)(\tfrac{1}{2}\tau_1 \tfrac{1}{2}\tau | T M_T)(\tfrac{1}{2}\tau_2 \tfrac{1}{2}\tau_3 | T M_T)\ \hat{l}\hat{j}\hat{j}_1\hat{j}_2\hat{j}_3 \\
& \times \sum_{LL''S} 3\delta_{S,1}(-)^{l+L}(\hat{L}\hat{L}'')^2 \begin{Bmatrix} l_1 & \frac{1}{2} & j_1 \\ l & \frac{1}{2} & j \\ L & S & J \end{Bmatrix} \begin{Bmatrix} l_2 & \frac{1}{2} & j_2 \\ l_3 & \frac{1}{2} & j_3 \\ L'' & S & J \end{Bmatrix} B_{LL''J}(i) \sum_{n_2' l_2' n_3' l_3'} A^{n_2' l_2' n_3' l_3' L''}_{n_2 l_2 n_3 l_3 L}(i)\, W(l_2' l_3' l_1 l : L'' L') \\
& \times \sum_{NL'N'\Lambda'n'l'} \langle n'l'N'\Lambda' : l | 2 : 1 | NL' n_3' l_3' : l \rangle \phi_{n'l'}\left(\frac{\gamma q}{\sqrt{3}}\right)(-)^{n'+(l'+\Lambda'+l)/2+L'+1}\ \hat{l}'\hat{L}'(l'0l|\Lambda'0) W(l_2 l_3 l_1 l; LL') \\
& \times \left[\sum_{\nu} \phi_{\nu 0}(0) \langle \nu 0 N L' : L' | 1 : 1 | n_1 l_1 n_2' l_2' : L' \rangle\right] \pi^{3/2} \int_0^\infty ds s^2 V^{(i)}_{ST}\left(\sqrt{\tfrac{3}{2}} s\right) j_{\Lambda'}\left(\sqrt{\tfrac{2}{3}}\gamma s q\right) \phi_{N'\Lambda'}(s), \qquad \text{(A5)}
\end{aligned}
$$

where $B_{LL''J}(\mathrm{so}) = W(1L1J; L''1)$ and

$$
A^{n_2' l_2' n_3' l_3' L''}_{n_2 l_2 n_3 l_3 L}(\mathrm{so}) = -\sum_{\nu\lambda N\Lambda} \sqrt{6\lambda(\lambda+1)(2\lambda+1)}\, W(1L\lambda\Lambda; L''\lambda) \langle \nu\lambda N\Lambda : L | 1 : 1 | n_2 l_2 n_3 l_3 : L \rangle \langle \nu\lambda N\Lambda : L'' | 1 : 1 | n_2' l_2' n_3' l_3' : L'' \rangle, \qquad \text{(A6)}
$$

while $B_{LL''J}(t) = W(L''2J1; L1)$ and

$$
A^{n_2' l_2' n_3' l_3' L''}_{n_2 l_2 n_3 l_3 L}(t) = 2\sqrt{30} \sum_{\nu\lambda N\Lambda\lambda''} \hat{\lambda}(\lambda 020|\lambda'' 0) W(2L\lambda''\Lambda; L''\lambda) \langle \nu\lambda N\Lambda : L | 1 : 1 | n_2 l_2 n_3 l_3 : L \rangle \langle \nu\lambda'' N\Lambda : L'' | 1 : 1 | n_2' l_2' n_3' l_3' : L'' \rangle \qquad \text{(A7)}
$$

for $i = \mathrm{t}$. The source term $U_{lj}(\xi)$ in the coordinate space is obtained then as

$$
U_{lj}(\xi) = -\frac{(\alpha+1)^{-3/2}}{2\pi^2} e^{\frac{\alpha\xi^2}{2b^2}} \int_0^\infty dq q^2 j_l(q\xi) e^{\beta q^2 b^2} U_{lj}(q), \qquad \text{(A8)}
$$

where ξ is the normalized Jacobi coordinate of the removed nucleon, $\alpha = (2A-1)^{-1}$, $\beta^{-1} = 8A(A-1)\alpha$, and $U_{lj}(q)$ is a linear combination of $U^{\alpha_1\alpha_2\alpha_3}_{ljm_j\tau}(q)$ with the weights determined by the effective shell model interactions.

[1] V. R. Pandharipande, I. Sick, and P. K. A. deWitt Huberts, Rev. Mod. Phys. **69**, 981 (1997).
[2] G. J. Kramer, H. P. Blok, and L. Lapikás, Nucl. Phys. A **679**, 267 (2001).
[3] J Lee, J. A. Tostevin, B. A. Brown, F. Delaunay, W. G. Lynch, M. J. Saelim, and M. B. Tsang, Phys. Rev. C **73**, 044608 (2006).
[4] A. Gade *et al.*, Phys. Rev. C **77**, 044306 (2008).
[5] B. P. Kay, J. P. Schiffer, and S. J. Freeman, Phys. Rev. Lett. **111**, 042502 (2013).
[6] M. B. Tsang, J. Lee, and W. G. Lynch, Phys. Rev. Lett. **95**, 222501 (2005).
[7] F. Flavigny, A. Obertelli, A. Bonaccorso, G. F. Grinyer, C. Louchart, L. Nalpas, and A. Signoracci, Phys. Rev. Lett. **108**, 252501 (2012).
[8] R. Shane *et al.*, Phys. Rev. C **85**, 064612 (2012).
[9] J. Lee *et al.*, Phys. Rev. Lett. **104**, 112701 (2010).
[10] F. Flavigny *et al.*, Phys. Rev. Lett. **110**, 122503 (2013).
[11] I. Brida, Steven C. Pieper, and R. B. Wiringa, Phys. Rev. C **84**, 024319 (2011).
[12] G. F. Grinyer *et al.*, Phys. Rev. Lett. **106**, 162502 (2011).
[13] G. F. Grinyer *et al.*, Phys. Rev. C **86**, 024315 (2012).
[14] O. Jensen, G. Hagen, M. Hjorth-Jensen, B. A. Brown, and A. Gade, Phys. Rev. Lett. **107**, 032501 (2011).
[15] C. Barbieri, Phys. Rev. Lett. **103**, 202502 (2009).
[16] C. Barbieri and W. H. Dickoff, Int. J. Mod. Phys. A **24**, 2060 (2009).
[17] N. K. Timofeyuk, Phys. Rev. Lett. **103**, 242501 (2009).
[18] N. K. Timofeyuk, Phys. Rev. C **81**, 064306 (2010).
[19] N. K. Timofeyuk, Phys. Rev. C **84**, 054313 (2011).
[20] N. K. Timofeyuk, Nucl. Phys. A **632**, 19 (1998).
[21] A. M. Mukhamedzhanov and A. S. Kadyrov, Phys. Rev. C **82**, 051601(R) (2010).
[22] L. D. Blokhintsev, I. Borbely, and E. I. Dolinskii, Sov. J. Part. Nuclei **8**, 485 (1977).
[23] C. W. De Jager, H. De Vries, and C. De Vries, At. Data Nucl. Data Tables **14**, 479 (1974).
[24] D. J. Millener, in *Topics in Strangeness Nuclear Physics*, Lecture Notes in Nuclear Physics, edited by P. Bydzovsky, A. Gal, and J. Mares (Springer, New York, 2007), Vol. 724, p. 31.
[25] G. Bertsch, J. Borysowicz, H. McManus, and W. G. Love, Nucl. Phys. A **284**, 399 (1977).
[26] J. P. Elliott, A. D. Jackson, H. A. Mavromatis, E. A. Sanderson, and B. Singh, Nucl. Phys. A **121**, 241 (1968).

[27] S. M. Bekbaev *et al*., Sov. J. Nucl. Phys. **54**, 232 (1991).
[28] R. B. Wiringa, http://www.phy.anl.gov/theory/research/overlap.
[29] I. R. Gulamov, A. M. Mukhamedzhanov, and G. K. Nie, Phys. At. Nucl. **58**, 1689 (1995).
[30] N. Burtebayev *et al*., Nucl. Phys. A **909**, 20 (2013).
[31] A. H. Wuosmaa *et al*., Phys. Rev. C **78**, 041302(R) (2008).
[32] S. V. Artemov *et al*., Bull. Rus. Acad. Sci. Physics **75**, 920 (2011).
[33] Z. H. Li *et al*., Nucl. Phys. A **834**, 661c (2010).
[34] B. Guo *et al*., Phys. Rev. C **87**, 015803 (2013).
[35] A. Banu *et al*., Phys. Rev. C **79**, 025805 (2009).
[36] S. V. Artemov, E. A. Zaparov, and G. K. Nie, Bull. Rus. Acad. Sci. Phys. **67**, 1741 (2003).
[37] A. M. Mukhamedzhanov *et al*., Phys. Rev. C **56**, 1302 (1997).
[38] K. M. Nollett and R. B. Wiringa, Phys. Rev. C **83**, 041001(R) (2011).
[39] P. Navratil, R. Roth, and S. Quaglioni, Phys. Lett. B **704**, 379 (2011).
[40] P. Descouvemont, Phys. Rev. C **70**, 065802 (2004).
[41] D. Baye and N. K. Timofeyuk, Phys. Lett. B **293**, 13 (1992).
[42] L. Lapikás, J. Wesseling, and R. B. Wiringa, Phys. Rev. Lett. **82**, 4404 (1999).
[43] R. C. Johnson and Tandy, Nucl. Phys. A **235**, 56 (1974).
[44] N. K. Timofeyuk and R. C. Johnson, Phys. Rev. Lett. **110**, 112501 (2013).
[45] N. K. Timofeyuk and R. C. Johnson, Phys. Rev. C **87**, 064610 (2013).
[46] M. Moshinsky and Yu. F. Smirnov, *The Harmonic Oscillator in Modern Physics* (Harwood Academic Publishers, Amsterdam, 1996).